HAL
open science

Analysis of non-thermal velocities in the solar corona

L. Contesse, S. Koutchmy, C. Viladrich

To cite this version:

L. Contesse, S. Koutchmy, C. Viladrich. Analysis of non-thermal velocities in the solar corona. Annales Geophysicae, 2004, 22 (8), pp.3055-3062. hal-00328969

HAL Id: hal-00328969

https://hal.science/hal-00328969v1

Submitted on 18 Jun 2008

HAL is a multi-disciplinary open access archive for the deposit and dissemination of scientific research documents, whether they are published or not. The documents may come from teaching and research institutions in France or abroad, or from public or private research centers.

L'archive ouverte pluridisciplinaire **HAL**, est destinée au dépôt et à la diffusion de documents scientifiques de niveau recherche, publiés ou non, émanant des établissements d'enseignement et de recherche français ou étrangers, des laboratoires publics ou privés.

Annales Geophysicae (2004) 22: 3055–3062
SRef-ID: 1432-0576/ag/2004-22-3055
© European Geosciences Union 2004

Annales Geophysicae

Analysis of non-thermal velocities in the solar corona

L. Contesse , S. Koutchmy , and C. Viladrich

Institut d'Astrophysique de Paris, 98 Bis Bd Arago, 75014 Paris, France

Received: 26 September 2003 – Revised: 22 April 2004 – Accepted: 12 May 2004 – Published: 7 September 2004

Abstract. We describe new ground-based spectroscopic observations made using a 40-cm aperture coronagraph over a whole range of radial distances (up to heights of 12′ above the limb) and along four different heliocentric directions N, E, S and W. The analysis is limited to the study of the brightest forbidden emission line of Fe XIV at 530.3 nm, in order to reach the best possible signal-to-noise ratio. To make the results statistically more significant, the extracted parameters are averaged over the whole length of the slit, and measurements are repeated fives times at each position; the corresponding dispersions in the results obtained along the slit are given. Central line profile intensities and full line widths (FWHM) are plotted and compared to measurements published by other authors closer to the limb. We found widths and turbulent (non-thermal) velocities of significantly higher values above the polar regions, especially when a coronal hole is present along the line of sight. We do not see a definitely decreasing behaviour of widths and turbulent velocities in equatorial directions for larger radial distances, as reported in the literature, although lower values are measured compared to the values in polar regions. The variation in the high corona is rather flat and a correlation diagram indicates that it is different for different regions and different radial distances. This seems to be the first analysis of the profiles of this coronal line, up to large heights above the limb for both equatorial and polar regions.

Key words. Magnetospheric physics (MHD waves and instabilities) – Space plasma physics (turbulence) – Solar physics (corona and transition region)

1 Introduction

Any measurement of non-thermal velocities distributed inside the coronal plasma is a good diagnostic for studying both the origin of the coronal heating and the sources of the solar wind (see, e.g. Doschek et al. 2001). Two mechanisms are today widely discussed to explain the high temperature of the corona (see, e.g. Phillips, 1995) and how it is maintained:

1. The dissipation of small-scale electric currents associated with a changing small-scale magnetic field, currently described by the concept of reconnection of magnetic field lines (see Priest and Forbes, 1999). Impulsive heating and sudden local release of energy leading to high temperature effects and transient brightenings are possibly the signature of this mechanism, (see, e.g. Smartt, Zhang and Smutko, 1993; Wood et al., 1998). We will not consider this process in this paper simply because it presumably requires good spatial resolution observations which are difficult to obtain simultaneously with precise spectroscopic data, especially from the ground. Another reason is that this mechanism certainly operates close to the surface and our coronagraphic observations are done well above the surface.

2. Nonlinear effects occurring during the propagation of waves inside a magnetically dominated atmosphere and further, in the outermost atmosphere where waves are guided. Waves obviously produce displacements, including unresolved proper motions which can better be studied by measuring Doppler effects seen in the broadened profiles of coronal emission lines. Because of the high level of structuring in the corona, as shown on high resolution coronal images, the observed broadening shows the integration effects along the line of sight. However, depending on the importance of waves, one can look for a signature at different heights, keeping in mind that the hydrostatic pressure scale (see November and Koutchmy, 1996) is of the order of 100 Mm in a 2×10^6 K corona (or two times less, in a presumably more inner 1×10^6 K corona). Observations usually have a spatial resolution significantly better than this scale, and their resolution is often comparable or similar to the typical scale of variations of the coronal magnetic field. Accordingly, we can expect some dispersion occurring in the real data when looking at an "instantaneous" line profile, even after integration along the line of sight, due to the finite number of summed contributions along the line of sight at a given moment of observation.

Correspondence to: S. Koutchmy
(koutchmy@iap.fr)

Another important aspect of the coronal dynamics is the outward acceleration of the "bulk" (magnetic) coronal plasma leading to the solar wind. Recent movies made using the beautiful LASCO observations from SoHO, amply demonstrated that a permanent flow with different scales, including the smallest one which is evidently not fully resolved, exists along streamers (movies are available on CDs by ESA and by NASA or using the Web sites of SoHO in USA or Europe). At larger scales, coronal mass ejections (CMEs) are episodically observed, but their study requires more global diagnostics. Here we will not discuss these phenomena any further.

We know for a long time that a solar wind of significantly larger speed originates more from coronal holes than from other regions of the Sun (the so-called fast wind is typically a factor of two faster than the slow wind). The mechanism(s) of acceleration operating at some unknown distance from the Sun, here again, is not clear. It has been suggested by several authors that waves outwardly propagating along an approximately radial magnetic field (presumably "open") could explain the strong wind coming from a large part of the corona (see, e.g. Wilhelm et al., 1998; Tziotziou et al. 1998; see also the recent review by Woo and Habbal, 2002 for an alternative topological configuration). The propagating waves in the corona are believed to have short periods and small amplitudes, just because, low in the corona, magnetic forces dominate pressure gradients of the high temperature (at least 10^6 K) plasma. Often Alfvén waves coupled with the plasma are suggested (see, e.g. Axford and McKenzie, 1992). They are difficult to resolve but their signature on the line profiles of strong emission lines should be imprinted; associated velocities are usually called non-thermal (or turbulent) velocities and they have been discussed for a long time since all coronal lines are indeed affected.

To perform a precise line profile analysis far enough out in the corona, the strongest emission line available, when using a Lyot ground-based coronagraph, the forbidden line of FeXIV at 530.285 nm, is the best choice. Note that this line produces a photon flux per resolution element several ten times larger than the strongest EUV lines, such as the Fe IX and XI lines at 17.1 nm used currently for coronal imaging from space. This truly coronal emission line is not sensitive to the so-called Doppler dimming effect (see, e.g. Kohl and Withbroe, 1982), such that its profile is directly reflecting line-of-sight velocities inside the corona. In addition, it has been established a long time ago (see Allen, 1946) that the line is measurable in the corona all along large radial distances (beyond at least three solar radii from the solar center). Accordingly, a detailed quantitative analysis of the line profiles can be made, even when using a temporal resolution of the order of 0.1 min (with the possibility to search for oscillations). As a rule, the signal-to-noise ratio is usually high enough to measure easily any departures from a Gaussian profile, and also to deduce some effective Doppler shifts from an average profile (see, e.g. Tsubaki, 1975 and Koutchmy et al., 1983) with a precision better than 1 km/s. Another advantage of this nearly 2×10^6 K line is that it is produced almost everywhere inside the corona and up to great heights (see Arnaud, 1982 for coronagraphic observations; Kim, 2000; Bocchialini and Koutchmy, 2001 for eclipse observations). Many observations were collected with coronagraphs, both photographically and photoelectrically. Well above the limb, especially in polar regions, the coronal signal obtained with a ground-based coronagraph becomes weak above the so-called aureola background parasitic light level. The use of a very sensitive and linear charge-coupled device (CCD) camera extended in dynamical range makes possible a new way to analyse the line by subtracting the background. Note that the limitation occurring in space due to the limited telemetry rate does not exist at ground-based sites.

Recently, Singh et al. (1999, 2002, 2003) published a series of new and well-documented papers devoted to the analysis of the main coronal lines observed using the Norikura Observatory Lyot coronagraph of 25-cm aperture. CCD spectra were obtained with high signal-to-noise ratio and the behaviour of the line broadening as a function of height was studied in particular. Impressive results were obtained, very similarly to the earlier classical study of Tsubaki (1975) made with the larger 40-cm aperture coronagraph at Sacramento Peak Observatory, but using photographic film of lower sensitivity. Surprisingly, Singh et al. did not find definite evidence for increasing amplitudes of non-thermal velocities in the Fe XIV line with height. Instead, they describe some decrease of non-thermal velocities measured from their line profile analysis, for heights up to 140′ above the limb. Note that this is still a rather limited range, not surpassing two hydrostatic scale heights. In addition, their study was limited to bright regions of the corona related to limb coronal enhancement probably overlying sunspots and facular regions.

Here we report similar measurements, but extended to much greater heights and using the larger diameter 40-cm coronagraph and an excellent 16-bit CCD camera. Depending of the parts of the corona under investigation, our results differ from those of Singh et al. We also consider weak polar coronal regions. It is the first time that a CCD analysis of line profiles is performed so far in the corona using the Fe XIV line.

Finally, it is important to mention that line profile analyses of resonance lines, like the HI Ly α line and the OVI doublet near 103 nm, performed with the UVCS instrument of SoHO, already provided strong evidence of very large effective ion temperatures above coronal holes (see, e.g. Cranmer, 2002). Additional effects could also be considered in terms of very large non-thermal velocities.

2 Observations

Observations that we collected used a setup located at the output of the universal spectrograph of the NSO-Sacramento Peak Observatory (at 2800 m elevation) coronagraph of 40-cm aperture. For a description of the facility, see http://nsosp.nso.edu/esf/userman/coronagraph.html. We performed a set

of observations extended over several weeks, but only the best data collected on 31 March 2002 are discussed here. Unfortunately, the EIT instrument of SoHO was not in operation at that time. In space only the EUV imaging instruments of the Russian Coronas spacecraft were collecting data. From the ground, we simultaneously obtained Hα slit-jaw images. They are of little scientific interest on their own, but could be used to check the position of the slit of the spectrograph, and also the sky brightness and viewing during our observations. However, many FeXIV images collected with the MIrror Coronagraph for Argentina (MICA) coronagraph operated in Argentina (Stenborg et al., 1999) are available for the day of observation (see Fig. 1).

We selected the best time of the day when the Sun was high enough (at least 30° above the horizon) to have a reduced atmospheric aureola background, as measured with the Evans' sky photometer of Sacramento Peak Observatory, but still before the hours of important heating due to solar irradiation, which generates large viewing effects in both the Earth's atmosphere and inside the coronagraph. Spectra were obtained between 15:30 and 18:00 UT on 31 March 2002. The 100 μm width slit, corresponding to 2″ on the sky, was put orthogonally to the local radial direction, at selected radial distances, r, and consecutively at different positions exactly above the N, E, S, and W limbs (see Fig. 1 and Table 1). We used a dispersion similar to what was used by Tsubabi (1975); other parameters, such as the setup after the exit of the spectrograph, were similar to what has been used by Koutchmy et al. (1983) with the same instrument to obtain photographic time sequences to search for FeXIV oscillations. The resulting spectral dispersion was 4.05 pm per pixel, taking into account the 9 μm pixel size of the Kodak KAF 1602E chip. After the re-imaging Micro-Nikkor lens and a field lens, an almost perfectly flat field over the whole chip was obtained (no trace of vignetting effect could be detected over the whole field). The adjusted effective exposure time was 5 s, just enough to avoid any saturation of the chip and to provide the best signal-to-noise ratio over a 16-bit dynamic range. The cosmetic property of the cooled chip at −20 C was found to be excellent, judging from different calibration spectra, including solar spectra taken with the diffuser put in the light path of the coronagraph. We accurately removed the bias and dark currents from each frame and for each selected position shown on Fig. 1. We consecutively recorded five frames in order to improve, after averaging the set, the signal-to-noise ratio over profiles which were extracted from the resulting images. Before averaging, individual spectra were co-aligned with a precision of 1/10 of a pixel in the spectral direction (note that the observed shifts of the overall spectra never exceeded one pixel for each set) and geometric distortion effects were removed. Regarding the other direction, note that the instrument uses a 4-quadrant-cell system of guiding to keep the same region on the slit during the recordings of each set of spectra, although the viewing is the real factor limiting the spatial resolution. An additional smearing is produced by the temporal averaging (typically 2-min averages).

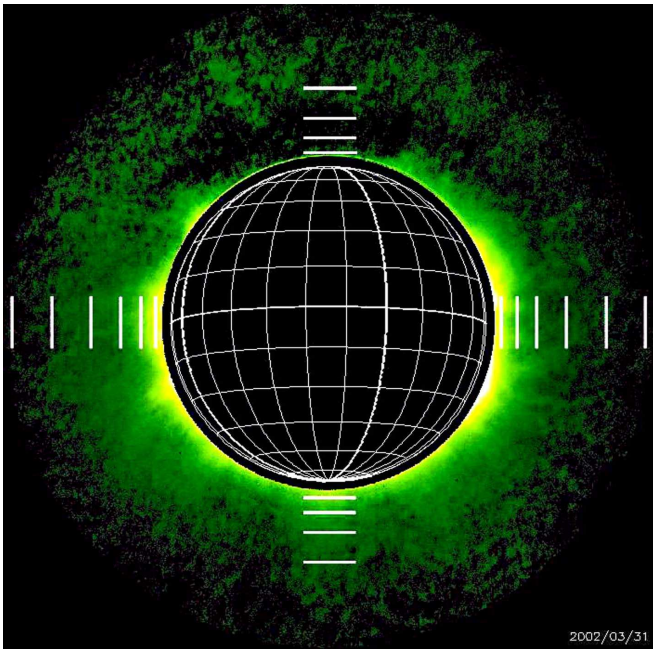

Fig. 1. A reconstructed image of the Fe XIV corona made from the series of observations with the MICA coronagraph in Argentina (see Stenborg et al., 1999). The positions and lengths of the entrance slit of our spectrograph are indicated (see also Table 1). The MICA image is a processed average of the best frames taken during the whole duration of our observations on 31 March 2002. Note the absence of a significant signal above the North Pole, which is a result of both the weak level of Fe XIV line emission and possibly of a slightly exaggerated cancellation of the (fluctuating) background.

A very important step in analysing the spectra is the removal of the background aureola parasitic light scattered inside the instrument, A_i(r), superposed on the light coming from the sky, A_s(r), which is mainly produced by the forward scattering by aerosols. The summed intensity corresponds to the intensity of the so-called aureola, which decreases drastically when going away from the limb. All components of the aureola are coming from the solar disk illumination and evidently contain all the Fraunhofer lines of the solar spectrum. We tried several methods for removing the background, including some convoluted spectra computed from the AFGL solar irradiance atlas of Sacramento Peak Observatory, using a spectral smearing function of slightly different widths. Finally, the best background cancellation was obtained using spectra taken before and after the series, over the aureola at a large radial distance (r>1.5 solar radius) in polar directions and normalizing each reference spectrum with the effectively measured intensity of the "continuum" near the coronal line. Figure 2 shows an example of an image of an observed average spectrum (no corrections) and the resulting emission line spectrum alone, after removing the background. Figure 3 is showing a display of all raw intensities of a background-subtracted spectrum collected from a slit position close to the limb. Interestingly, a very small effect is still detectable in the residual background level due to an imperfect cancellation.

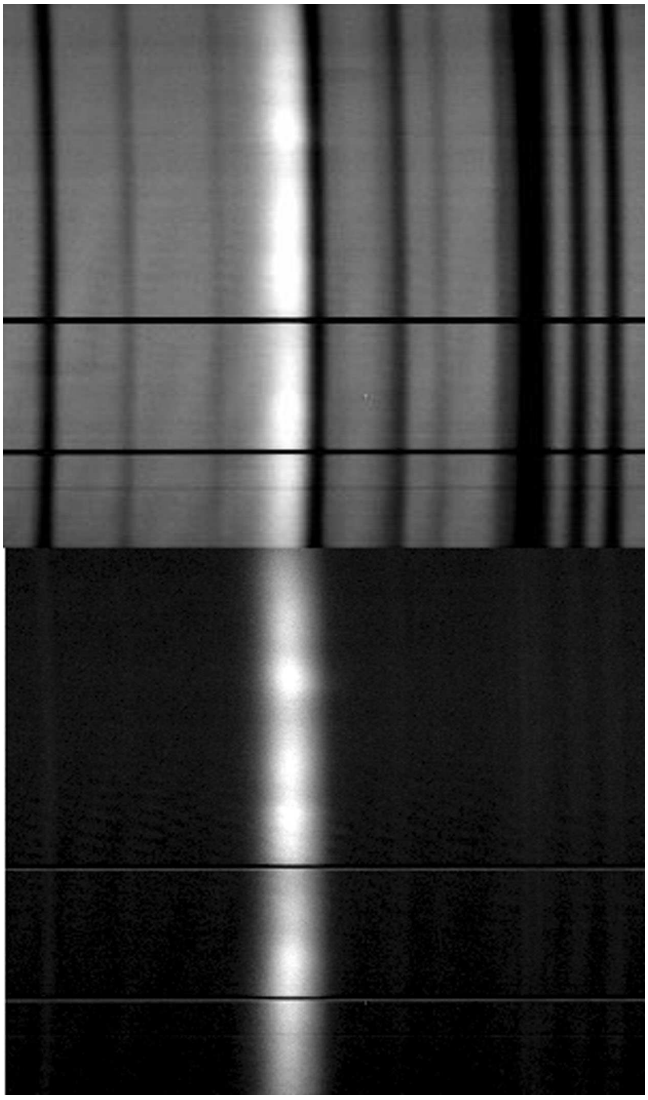

Fig. 2. Average image of the spectrum taken above the E-limb at a distance of 1.5′ from the limb (this position of the slit is barely seen in Fig. 1). At the top, a raw spectrum; at the bottom, the coronal spectrum after removing the parasitic background light and correcting the spectrum for geometric distortion effects. Note the rather large inhomogeneities of coronal line emissions along the length of the slit. The hair lines are also kept (two dark lines crossing the spectra) to show a distance of 56 Mm in the corona along the slit.

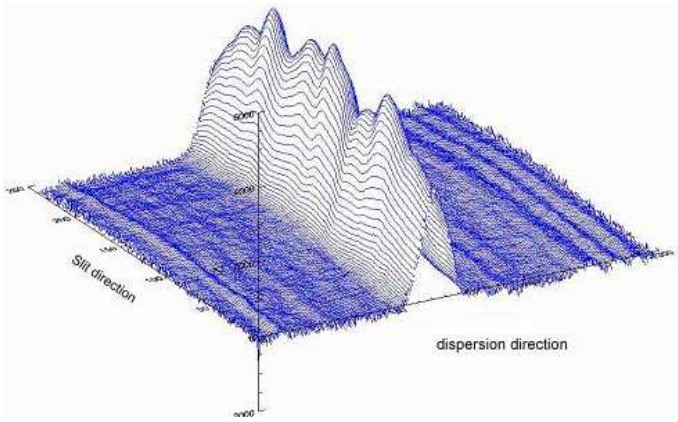

Fig. 3. Three-dimensional display of the distribution of the Fe XIV emission line profiles along the slit, after removing the background and hair lines and averaging five spectra. Note the variations in the central intensities. The slit was put at an average height of 1.5′ from the east limb.

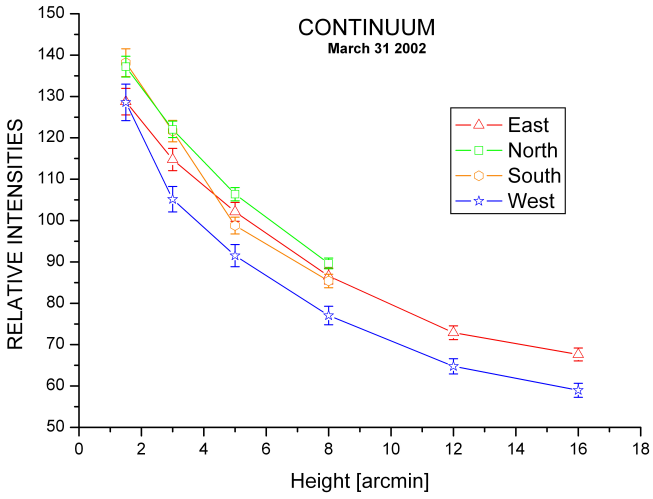

Fig. 4. Radial variations of the average intensities of the aureola background measured in the neighbouring continuum of the coronal line at 530.3 nm. Time of the day when the data are collected are shown in Table 1. Accordingly, the Earth's atmospheric component of the aureola changes by a small amount. Intensities are given in units of 10^{-6} of the average brightness of the solar disk.

This is just because the radial variation of the intensity of the aureola is stronger close to the limb than at a large radial distance, where the reference background spectra are made, using the same slit length (see Fig. 1). In Fig. 4, we show the intensity of the aureola measured in a spectral window corresponding to the continuum near 530.3 nm, at different times (see Table 1) and different directions. Intensities integrated along the line of sight were converted in absolute units of the average intensity of the solar disk at the same wavelength, as usually done by coronagraphic observers. We see that near the limb, intensities reach rather high values (keep in mind, however, that the Sun was not at its highest elevation in the sky). Different methods were tried to deduce these absolute values and a fair agreement is indeed obtained with the scale of brightnesses of FeXIV used at Sacramento Peak Observatory when the photoelectric coronal emission lines photometer is used to perform routine measurements.

3 Results of the analysis

After subtracting the background, we obtain the full line profiles which still have to be corrected for the instrumental broadening, using the usual method where the instrumental

Table 1. Times, positions and numbers of the analysed slit spectra (see Fig. 1).

West Limb:		East Limb:	
t_{start}: 15:34 UTC		t_{start}: 15:50 UTC	
Minutes of arc from the limb		Minutes of arc from the limb	
W1 to 5	1.5	E4 to 8	1.5
W6 to 10	3	E9 to 13	3
W11 to 15	5	E14 to 18	5
W16 to 20	8	E19 to 23	8
W21 to 25	12	E24 to 28	12
W26 to 30	16	E29 to 33	16
North Limb:		South Limb:	
t_{start}: 16:10 UTC		t_{start}: 16:52 UTC	
Minutes of arc from the limb		Minutes of arc from the limb	
N1 to 5	1.5	S1 to 5	1.5
N6 to 10	3	S6 to 10	3
N11 to 15	5	S11 to 15	5
N16 to 20	8	S16 to 20	8

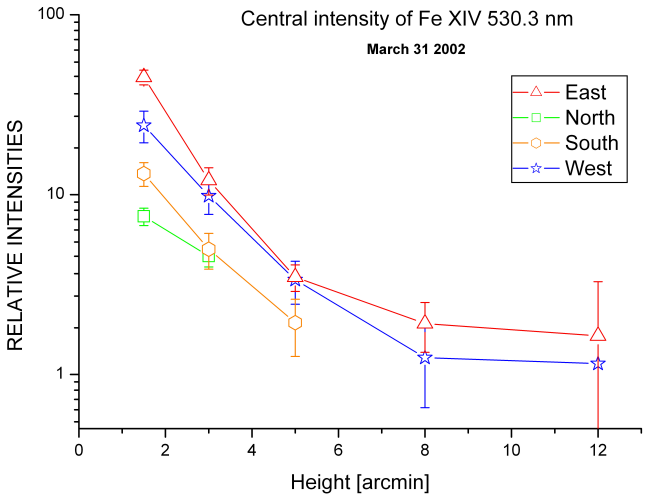

Fig. 5. Radial variations of the 530.3-nm Fe XIV coronal central line average intensities for different directions (see Fig. 1). Units are the same as in Fig. 4 and intensities are averaged over the whole length of the slit shown in Fig. 1. Bars of uncertainty correspond to the dispersion of the intensities measured over the length of the slit; the level of the noise is always smaller.

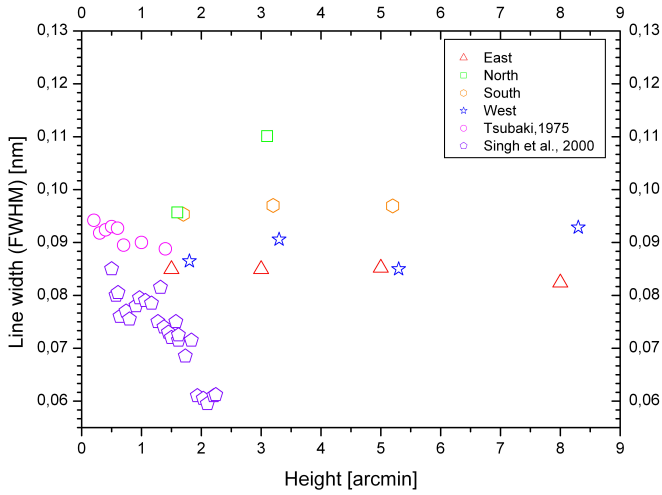

Fig. 6. Variations of the line widths as a function of height above the limb for different directions shown in Fig. 1 of this paper, and above coronal enhancement regions, as reported by Tsubaki (1975) and also, for selected regions, by Singh et al. (2000).

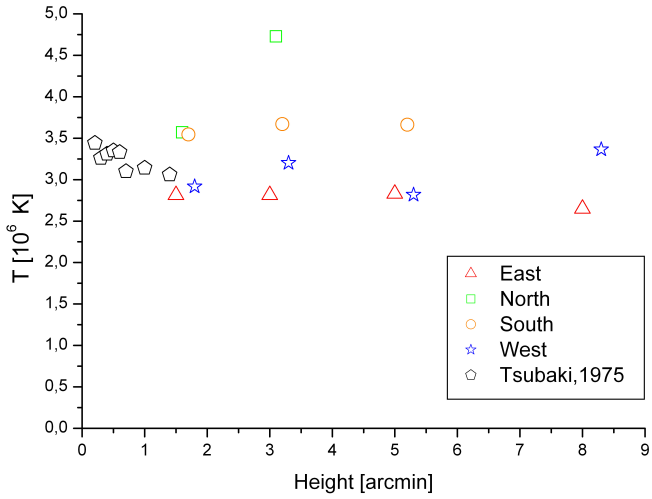

Fig. 7. As in Fig. 6, but now considering the Doppler temperatures (effective ion temperatures) computed from the line widths. Note the excellent agreement with the Tsubaki (1975) values when considering the same radial distances and only equatorial regions.

profile is assumed to be of Gaussian shape. Furthermore, all line profiles were fitted with a simple Gaussian, a procedure which leads to some small dispersion (see Table 2) but provides a precise comparison with data coming from other published analyses. The deduced central intensities of the line are plotted as a function of radial distances in Fig. 5, showing mutually consistent data sets, with the coronagraphic data obtained by Arnaud (1982) at Pic du Midi Observatory. Note that even north, where a coronal hole is possibly situated along the line of sight (see Fig. 1), we measured a substantial level, probably because we cross at least some boundaries of the hole: polar holes are not covering the whole polar region at this time of the solar cycle (typically one year after the sunspot maximum). This is confirmed by studying the polar regions from the EIT Fe XV images taken before and after our observations (not shown here), as well as by looking at the images taken on 17 March and 14 April 2002, which correspond to the corona seen behind the limb but are still relevant for a line of sight integration above

Table 2. Average for each slit length of the measured parameters of FeXIV line emissions in different locations of the solar corona (see Fig. 1). We did not report all the analysed data (see Table 1), in order to keep a good enough signal-to-noise ratio, which means that very low level emissions are not discussed here.

	Height above the limb [arcmin]	Average Central Intensities	Min	Max	FWHM [pm]	Dispersion of FWHM [pm]	Dispersion in Doppler Shift [km/s]
	1.5	45.0	34.3	52.9	84.9	1.37	2.61
	3	12.0	7.6	15.8	84.9	1.67	3.80
East	5	3.5	2.3	5.0	85.2	4.25	3.51
	8	1.9	0.0	3.2	82.4	6.97	1.94
	12	1.6	0.0	2.8	105.8		
1.5	24.3	13.9	39.7	86.5	4.67	4.03	
	3	9.8	6.6	15.6	90.6	7.35	3.40
West	5	3.4	1.0	5.3	85	4.71	3.33
	8	1.2	0.0	3.1	92.9	6.15	3.35
	1.5	7.6	4.9	9.7	95.7	3.92	3.27
North	3	4.6	3.0	6.4	110.1	4.32	4.96
1.5	13.1	6.9	16.3	95.3	4.11	3.46	
South	3	5.0	1.8	7.5	97	13.36	2.55
	5	1.9	0.0	3.5	96.9	11.43	2.94

the polar regions. So observations are not necessarily indicative of coronal hole conditions, at least at low heights, as confirmed by the examination of the 19.4-nm filtergram taken at the same time on Coronas [1].

The fitting of line profiles and the computation of their FWHM has been well described by Tsubaki (1975) and recently by Kim (2000) and again by the Singh et al. (1999, 2002, 2003), such that we do not consider it useful to repeat or duplicate here this part. The same is true for the extraction of the Doppler temperature, T_D, and of the turbulent velocities, V_t, making the assumption that the full profile is due to the superposition of thermal velocities at the formation temperature of Fe XIV, T_i , and to unresolved turbulent and isotropic velocities V_t, (also called non-thermal velocities), smearing the profiles integrated along each line of sight. Assuming that T_i is known from the ionisation balance calculations, and taking 55.85 for the atomic mass number of the Fe 13+ ions responsible for producing the Fe XIV line, it is easy to deduce a quite simple and practical formula relating the different parameters:

$$V_t = 17.2\,\mathrm{km/s}(T_D/\mathrm{MK} - T_i/\mathrm{MK})^{1/2}\,. \quad (1)$$

We take T_i=1.8 MK, i.e. to be equal to the temperature of maximum ionic fraction from Arnaud and Rothenflug, 1985. The measurements show that T_D never reaches a value under 1.8 MK, which corresponds to a FWHM of 0.068 nm (see Kim, 2000).

Figures 6 and 7 indicate the radial variations of the obtained average values of the FWHM and of the corresponding Doppler temperatures in all directions N, E, S, and W.

Finally, we plotted in Fig. 8 the computed turbulent velocities, assuming T_i=1.8 MK. The indicated uncertainties give the whole range of velocities we obtained for each position of the slit, which means the dispersion and not intrinsic uncertainties in measurements which are significantly lower.

4 Discussion of results

The first interesting result concerns the agreement we see with the Tsubaki (1975) photographic results, and, to some extent, with the Singh et al. (1999, 2002, 2003) results (see Fig. 6), taking into account that these authors studied the line profiles in specific regions, at low latitudes and for a rather limited extension in height. The results that we obtained over the polar regions cannot be compared with other ground-based coronagraphic data, because to our knowledge, there are no such observations. Regarding these regions, Figs. 6 and 7 show definitely larger values of both the widths and T_D. The effect can especially be seen above the north polar region, where intensities are, however, very low and correspondingly, the signal-to-noise level is lower. The effect is even better seen in the turbulent (non-thermal) velocities (see

[1] V. Slemzin and the Lebedev Institute team, private communication

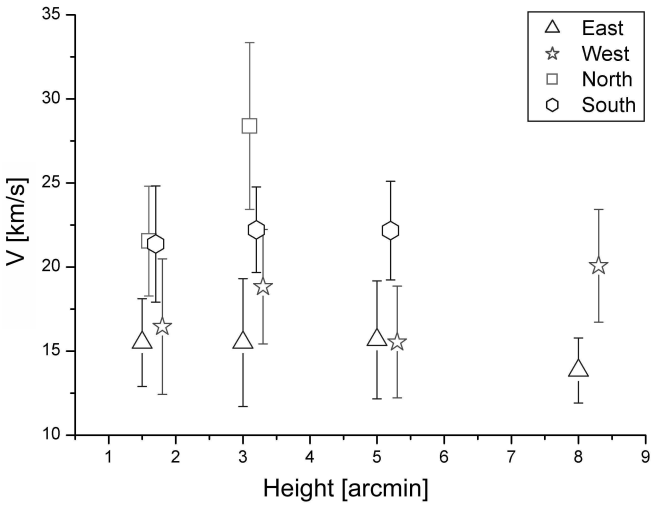

Fig. 8. Radial variations of the turbulent (non-thermal) isotropic velocities, assuming a temperature of 1.8 MK for the Fe XIV ions. Uncertainty bars correspond to the dispersion obtained along each slit length, not to the significantly smaller intrinsic uncertainties.

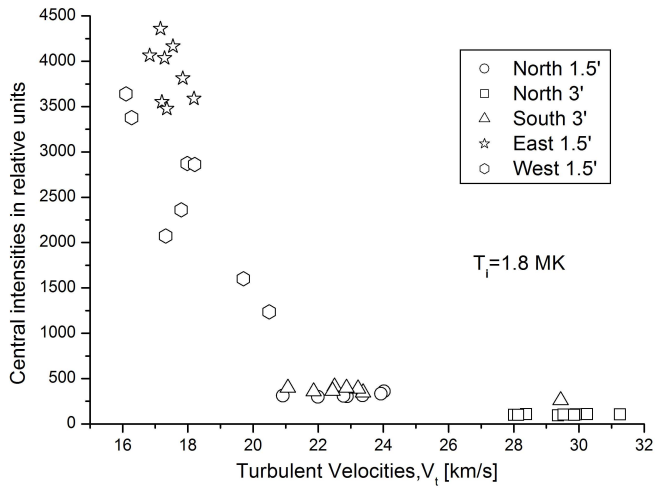

Fig. 9. Correlation plot between central intensities of each average Fe XIV line profile and the corresponding turbulent velocities. It shows different velocities V_t, depending on the distance from the limb (for polar regions only) and, in particular, on the latitudes of the emission and the brightness.

Fig. 8). This seems to tell us something about the coronal holes and coronal hole boundaries physics. SUMER/SoHO results of Wilhelm et al. (1998) are going in the same direction; we think our result is the first independent confirmation coming from CCD measurements on a forbidden line and FeXIV. Note that the more recent results of O'Shea, Banerjee and Poedts (2003) obtained using the MgX line observed with CDS/SoHO in a CH is more difficult to evaluate. Although in the more inner corona situated under 65 Mm, their reported data seems to support the behaviour of an increasing FWHM with heights, they see a different behaviour between 65 Mm and their maximum height of analysis situated at 90 Mm. It could be very important to continue these ground-based coronagraphic measurements further in the solar cycle, going to the minimum-type corona. Further out in the polar region corona, Hassler et al. (1990) and Kohl et al. (1999) reported space-borne results that were also in agreement with us. As far as eclipse results are concerned, we finally found the agreement to be excellent with data reported by Kim (2000).

Another type of diagnostics which we will now discuss concerns the behaviour of the coronal line widths, and, correspondingly, of turbulent (non-thermal) velocities for larger radial distances (or heights above the limb) in the equatorial regions. Our Figures 6, 7 and 8 do not confirm the very recent results by Singh et al. for particular regions. They found decreasing and rather small line-width values obtained near 2′ from the limb. Our data probably cover a larger average but, more importantly, we looked much further out in the corona,where we never see such narrow widths. Indeed, in the west, we have an almost flat or very slight increasing behaviour and, in the east, a very slight decreasing part. Some dispersion is, of course, present in the data (see also Table 2), but no indication of a systematic decrease in the widths would appear. To go further in the analysis of the discrepancy, we built a correlation diagram (see Fig. 9). The typical intensities of the line studied in the regions selected by Singh et al. correspond to intensities situated at the top of the diagram (the highest intensities corresponding to equatorial regions and to the position of the slit close to the limb). The highest intensities give the smallest values of turbulent velocities, in agreement with Singh and et al. (1999), and only for low intensities did we see a completely different behaviour, with high values of turbulent velocities occurring in these regions. This range of small intensities is obviously beyond the intensities used by Singh et al. (1999) and this is probably the origin of the apparent discrepancy. In polar regions, we think that there is no discrepancy and the observed line broadening is an argument in favour of coronal wave activity.

Acknowledgements. Data used in this paper were collected at NSO-Sacramento Peak Observatory sponsored by AURA and the US Air Force Research Labs. We thank the telescope allocation committee for the generous allocation of the time of the 40 cm coronagraph and especially R.C. Altrock, K. Balasubramaniam, R. N. Smartt, S. Hegwer and J. Cornett for their precious advices and help; L. Gilliams assisted us during the whole run and special thanks go to him. We are indebted to J-P. Maillard, J. Singh, R.N. Smartt, R. Taillet and K. Wilhelm for reviewing the first manuscript and to both our Referees for significantly improving it.

Topical Editor R. Forsyth thanks S. Fineshi and another referee for their help in evaluating this paper.

References

Allen, C. W.: The Spectrum of the Corona at the Eclipse of 1940, MN RAS, 106, 139, 1946.

Axford, C. W. and McKenzie, J. F.: In Solar Wind Seven, edited by Marsch, E. and Schwenn, R., Oxford: Pergamon Press, 1, 1992.

Arnaud, J.: Observed Polarization of the Fe XIV 5303 Coronal Emission Line, Astron. Astrophys. 112, 350–354, 1982.

Arnaud, M. and Rothenflug, R.: An Updated Evaluation of Recombination and Ionization Rates, Astron. Astrophys. Suppl. Series, 60, 425–457, 1985.

Bocchialini, K. and Koutchmy, S.: Analysis of Fe XIV Line Profiles to Search for Waves, Observations et Travaux, SAF Ed., 53, 60–62, 2001.

Cranmer, S. R.: Coronal Holes and the High-speed Solar Wind, Space Science Rev., 101, 229–294, 2002.

Doschek, G. A., Feldman, U., Laming, J. M., Schuhle, U., and Wilhelm, K.: Properties of Solar Polar Coronal Hole Plasmas Observed above the Limb, Astrophys. J., 546, 559–568, 2001.

Hassler, D. M., Rottman, G. J., Shoub, E. C., and Holzer, T. E.: Line broadening of Mg X 609 and 625 A coronal emission lines observed above the solar limb, Astrophys. J., 348, L77, 1990.

Kim, I. S.: Eclipse Spectra of the Coronal Velocity Field, in: The Last Total Solar Eclipse of the Millennium in Turkey, ASP Conf. Series, Vol. 205, 69–82, 2000.

Kohl, J. and Withbroe, G.: EUV spectroscopic plasma diagnostics for the solar wind acceleration region, Astrophys. J., 256, 263, 1982.

Kohl, J. L., Esser, R., Cranmer, S. R., Fineschi, S., Gardner, L. D., Panasyuk, A. V., Strachan, L., Suleiman, R. M., Frazin, R. A., and Noci, G.: EUV Spectral Line Profiles in Polar Coronal Holes from 1.3 to 3.0 R_solar, Astrophys. J., 510, L59, 1999.

Koutchmy, S., Zhugzda, Y. D., and Locans, V.: Short Period Coronal Oscillations: Observation and Interpretation, Astron. Astrophys. 120, 185–191, 1983.

November, L. and Koutchmy, S.: White-Light Coronal Dark Threads and Density Fine Structure, Astrophys. J., 466, 512–528, 1996.

O'Shea, E., Banerjee, D. and Poedts, S.: Variation of coronal line widths on and off the disk, Astron. Astrophys. 400, 1065–1070, 2003.

Phillips, K. J. H.: Guide to the Sun, Cambridge University Press, Cambridge, 1995.

Phillips, K. J. H., Read, P. D., Gallagher, P. T., et al.: SECIS: The Solar Eclipse Coronal Imaging System, Solar Phys. 193, 259–271, 2000.

Priest, E. R. and Forbes, T. G.: Magnetic Reconnection, Cambridge University Press, Cambridge, 1999.

Singh, J., Ichimoto, K., Imai, H., Sakurai, T., and Takeda, A.: Spectroscopic Studies of the Solar Corona, I. Spatial Variation in Line Parameters of Green and Red Lines, PASJ, 51, 269, 1999.

Singh, J., Sakurai, T., Ichimoto, K., Suematsa, Y., and Takeda, A.: Spectroscopic Studies of the Solar Corona, II. Proprieties of Green and Red Emission Lines in Open and Closed Coronal Structure, PASJ, 54, 793, 2002.

Singh, J., Ichimoto, K., Sakurai, T., and Muneer, S.: Spectroscopic Studies of the Solar Corona, IV. Physical Proprieties of Coronal Structure, Astrophys. J., 585, 516–523, 2003.

Smartt, R. N., Zhang, Z., and Smutko, M. F.: Post-Flare Coronal Loop Interaction, Solar Phys. 148, 139, 1993.

Stenborg, G., Schwenn, R., Srivastava, N., Inhester, B., Podlipnik, B., Rovira, M., and Francile, C.: The mirror coronagraph for Argentina, Space Sci. Rev., 87, 307, 1999.

Tsubaki, T.: Line Profile Analysis of a Coronal Formation Observed near a Quiescent Prominence, Solar Phys. 43, 147–175, 1975.

Tziotziou, K., Martens, P. C. H., and Hearn, A. G.: Energy and Momentum Deposition in Coronal Holes, Astron. Astrophys. 340, 203–215, 1998.

Wilhelm, K., Marsch, E., Dwivedi, B. N., et al.: The Solar Corona above Polar Coronal Holes as seen by SUMER on SoHO, Astrophys. J., 500, 1023–1038, 1998.

Woo, R. and Habbal, S. R.: The Origin of the Solar Wind, American Scientist, Vol. 90, 6, 532–539, 2002.

Wood, B. E., Karovska, M., Cook, J. W., Brueckner, G. E., Howard, R. A., Korendyke, C. M., and Socker, D. G.: Search for Brightness Variations in Fe XIV Coronagraph Observations, Astrophys. J., 505, 432–442, 1998.